Journal of Photochemistry and Photobiology A: Chemistry 216 (2010) 167–178

Contents lists available at ScienceDirect

Journal of Photochemistry and Photobiology A: Chemistry

journal homepage: www.elsevier.com/locate/jphotochem

Titania-containing mesoporous silica powders: Structural properties and photocatalytic activity towards isopropanol degradation

Minoo Tasbihi[a], Urška Lavrenčič Štangar[a,*], Andrijana Sever Škapin[b], Alenka Ristić[c], Venčeslav Kaučič[c,d], Nataša Novak Tušar[c,a]

[a] Laboratory for Environmental Research, University of Nova Gorica, Vipavska 13, 5001 Nova Gorica, Slovenia
[b] Slovenian National Building and Civil Engineering Institute, Dimičeva 12, 1000 Ljubljana, Slovenia
[c] Laboratory for Inorganic Chemistry and Technology, National Institute of Chemistry, Hajdrihova 19, 1000 Ljubljana, Slovenia
[d] Faculty for Chemistry and Chemical Technology, University of Ljubljana, Aškerčeva 5, 1000 Ljubljana, Slovenia

ARTICLE INFO

Article history:
Available online 15 July 2010

Keywords:
Mesoporous silica
Photocatalyst
Titanium dioxide
Isopropanol

ABSTRACT

Ordered (SBA-15) and disordered (KIL-2) mesoporous silica supports have been synthesized and used for incorporation of titania with different Ti/Si molar ratios (1/2, 1/1, 2/1) via sol–gel impregnation method. Titanium isopropoxide and aqueous titania sol prepared by low-temperature sol–gel processing were used as a source of titania. Characterization by powder X-ray diffraction (XRD), nitrogen sorption measurements, scanning electron microscopy (SEM) and UV–vis–NIR diffuse reflectance spectroscopy (DRS) has been carried out to investigate the chemical framework and morphology of powders. The photocatalytic degradation of isopropanol in the gaseous medium was selected as a probe reaction to test the photoactivity of powders and to verify the potential application of these materials for air remediation. It was found that the titania source, Ti/Si molar ratio and the type of silica support influenced the functional properties of the material, which were evaluated by adsorption capacity and photocatalytic activity in the gas–solid reactor. The adsorption capacity of isopropanol was the highest in the presence of the SBA-15-supported materials. The photoactivity results indicated that the powders which were prepared using SBA-15 as a silica support and a Ti/Si molar ratio of 1/1 were the most active towards isopropanol oxidation monitored in situ by FT-IR spectroscopy.

1. Introduction

The Mobil Corporation reported a series of ordered mesoporous silicates designated as M41S [1] that were synthesized by using a surfactant templating approach in the early 1990s and ever since much effort has been devoted to study the syntheses and applications of ordered mesoporous materials [2]. In 1988, Zhao et al. [3] synthesized SBA-15 mesoporous silica having a hexagonal structure with uniform tubular channels (50–300 Å), larger pore diameter and thicker walls in comparison to other mesoporous silicates such as MCM-41 and HMS [4–7]. Recently several studies of plugged mesoporous silica materials which are more stable than SBA-15 have been reported [8–14]. In 2000, plugged hexagonally templated silica (PHTS) containing extra microporous silica plugs in the mesoporous channels was synthesized by increasing the silica/surfactant ratio [14]. PHTS has the same 2D hexagonal symmetry as SBA-15, but some of its cylindrical mesopores have internal porous plugs, while others are open as inferred from gas adsorption–desorption data. Because of the pillared effect of the amorphous microporous nanoparticles, PHTS materials show a higher hydrothermal and mechanical stability compared to other mesoporous materials including pure SBA-15 [8–12]. Activation of meso-ordered silica material with different metals or metal oxides is contributing to the development and design of high surface area catalysts allowing high diffusion rates with improved catalytic activity for bulky molecules [15–29].

Titanium dioxide (TiO_2) is the well-known photocatalyst for decomposing organic pollutants in water and air [19]. Titanium dioxide can be incorporated in the silicate host by a post-synthesis method. Although the silica surface is relatively inert and it is hard to synthesize highly dispersed metal oxides on the silica surface, the surface silanols can serve as adsorptive and reactive sites. The titanium tetrachloride and titanium alkoxides can be used as sources of titanium reacting with the surface silanols [20]. The most facile and common methods involve incipient-wetness impregnation [16,17,21] and the grafting method [22,24–26]. For example Luan et al. [17,21] incorporated titania into mesoporous silica molecular sieve SBA-15 via incipient-wetness impregnation with various stoichiometric Si/Ti molar ratios in the range from 1 to 80. The results show that titania is present in two distinct chemical forms and their

* Corresponding author. Tel.: +386 5 331 52 41; fax: +386 5 331 52 96.
E-mail address: urska.lavrencic@ung.si (U.L. Štangar).

1010-6030/$ – see front matter © 2010 Elsevier B.V. All rights reserved.
doi:10.1016/j.jphotochem.2010.07.011

relative amounts depend on the titania loading. At low loading, the guest Ti-phase is monoatomically dispersed as titanium ions on the SBA-15 wall surface and the pore size of SBA-15 is not altered, whereas at high titanium loading a thin titanium dioxide anatase film is formed anchored inside the mesopores of SBA-15. Landau et al. [28] inserted TiO_2 (30–80 wt.%) inside the pores of SBA-15, with the minimum pore blocking, by chemical solution decomposition and internal hydrolysis. Both methods yielded composites with high (85–94%) TiO_2-anatase crystallinity. The nanocrystalline structure of TiO_2/SBA-15 composites did not change by calcination up to 800 °C while the crystal domain size increased slightly. Wang and Song [29] incorporated a high amount of titania into the mesoporous SBA-15 by employing a multistep impregnation method. They found very small titania nanodomains up to 1.3 nm in size instead of bulk titania phases. They suggested that a multistep impregnation method is more effective to incorporate high amount of titania compared to a one-step impregnation method. Perathoner et al. [22] studied the characteristics of TiO_2/SBA-15 materials with loading of TiO_2 below 15 wt.%. The SBA-15 was grafted with Ti-isopropoxide in different organic solvents. They found out that the pre-heating of the SBA-15 at 80 °C for 3 h or in more severe conditions at 140 °C for 12 h before the grafting with titania has some influence on the relative distribution of various titania species, affecting the concentration of hydroxyl groups and of defects. However, their results indicate that this could be considered as a minor effect. They confirmed that upon introduction by grafting, titanium compound reacts with silanol groups in the corona area of inner SBA-15 walls forming either TiO_4 tetrahedral sites and/or pseudo-octahedral surface sites anchored by two (or more) Si or Ti ions through bridging oxygen. In the region of high silanol density, where the micropores are located in the corona of SBA-15 channels, this reaction leads to the formation of TiO_2-like nanoareas with dimensions of around 1–2 nm not detected by XRD, but evidenced from the UV–vis spectroscopy. Their characterization results showed that there is no formation of a separate anatase phase and the distribution of Ti within the samples is homogeneous. Busuioc et al. [15] synthesized TiO_2/SBA-15 by the post synthesis deposition using the acid-catalyzed sol–gel method. They showed that by changing the initial amount of Ti-isopropoxide, pH and temperature for formation of TiO_2 sol, the size, the location and the amount of the anatase nanoparticles on SBA-15 could be controlled. By confining TiO_2 nanoparticles into SBA-15 the growth of these nanoparticles is controlled and the size could be tuned to within a few nanometers, resulting in an improved adsorption capacity and photocatalytic activity towards photodecomposition of rhodamine 6G in aqueous solution as compared with pure TiO_2.

In our previous work, the anatase-TiO_2 powders were prepared using titanium tetrachloride as a precursor via sol–gel method at low-temperature synthesis conditions [30]. Perchloric acid ($HClO_4$) and nitric acid (HNO_3) were used as peptizing mediators and $[Ti]/[H^+]$ ratios were fixed at 0.5 and 2.5. The TiO_2 sol was prepared after refluxing treatment at 70 °C for 24 h. The as-prepared anatase-TiO_2 sol was an acidic colloidal solution without any significant precipitation upon aging. The TiO_2 powders were obtained with consequent drying of the sols. The purpose was to get the powder which after the dissolution in water results in a stable colloidal solution (no precipitation) with the smallest possible aggregated particles. The titania particle sizes in the $HClO_4$-based sol were approximately two times smaller than those in the HNO_3-based sol. Furthermore, the specific surface area of $HClO_4$-prepared samples was approximately two times higher than that of the HNO_3-prepared samples, with the same $[Ti]/[H^+]$ ratio. So using $HClO_4$ instead of HNO_3 results in smaller colloidal particles of TiO_2 in the sol and in higher surface area of the powder, while the primary crystallite sizes for both types of powder are similar. Thus we concluded that perchloric acid has better peptizing characteristics than nitric acid, because it results in solutions with fewer aggregated particles.

The aggregation of the nanocrystallites often prevents a high catalytic activity. In this study, we used mesoporous silicates as a high surface area support to eventually prevent the aggregation of the TiO_2 powders. We synthesized ordered mesoporous SBA-15 and disordered mesoporous KIL-2 silicate materials. The KIL family is related to mesostructured silicate families with textural (interparticle) porosity (HMS, MSU, NBS) [31]. KIL-2 possesses interparticle mesopores with the pore dimensions from 5 to 60 nm and surface area of around 500 $m^2\,g^{-1}$. The mesopores are formed by the aggregation of silica nanoparticles thus creating the network with interparticle voids [31]. Two synthetic approaches were used to incorporate titania within the silica mesoporous materials starting from (i) titanium isopropoxide and (ii) aqueous crystalline titania sol, both as a source of titania to be incorporated in mesoporous silica. TiO_2 sol prepared by low-temperature sol–gel processing as described above with $HClO_4$ peptizing mediator ($[Ti]/[H^+] = 2.5$) was used in the latter approach. Titania was incorporated onto/into mesoporous silica in different Ti/Si molar ratios (1/2, 1/1, 2/1). The structural parameters and morphology of powders were characterized by X-ray diffraction (XRD), nitrogen sorption measurements, scanning electron microscopy (SEM) and UV–vis diffuse reflectance spectroscopy (DRS). We were interested in how the titania source and the type of silica support (ordered mesoporous SBA-15 type and a disordered mesoporous KIL-2 type) influenced the functional properties of the material, which were evaluated by measuring adsorption capacity and photocatalytic activity towards the photocatalytic degradation of isopropanol in a gaseous photocatalytic reactor.

2. Experimental

2.1. Synthesis of supporting silica materials

2.1.1. Synthesis of KIL-2

The two-step synthesis of the disordered mesoporous KIL-2 [31] powders was developed on the basis of the neutral templating method in which small, non-surfactant templates such as triethanolamine (TEA) direct the polycondensation of inorganic species. In the first step tetraethyl orthosilicate (TEOS) and triethanolamine were stirred for 30 min. Then deionized water was added to the mixture, followed by the addition of tetraethylammonium hydroxide (TEAOH). The solution was mixed with the aid of a magnetic stirrer to obtain homogeneous gel. The final gel, having pH of 7, with molar composition of 1 TEOS:0.5 TEA:0.1 TEAOH:11 H_2O was aged overnight at room temperature and then dried in an oven for 24 h at 50 °C. In the second step the gel was solvothermally treated in ethanol in Teflon-lined stainless steel autoclaves at 150 °C for 48 h. Removal of the template was performed by calcination at 500 °C for 10 h using a heating rate of 1 °C min^{-1} in air. In this way the thermal stability of the product was also established. The hydrothermal stability of the products was verified by keeping them in the boiling water for 2 h [31].

2.1.2. Synthesis of SBA-15

Ordered mesoporous silica SBA-15 powders were synthesized according to the well-known procedure [3,16]. 8 g of Pluronic® P123 triblock copolymer was added to 260 mL of distilled water and 40 mL of concentrated hydrochloric acid (37 wt.%, HCl). The mixture was stirred until the surfactant was dissolved. Then 17 mL of TEOS was added under stirring at 45 °C. The reaction gel was stirred for 8 h at 45 °C and aged for another 16 h at 80 °C. The obtained gel with molar ratios of reaction components 1 SiO_2:0.017 P123:5.85 HCl:190 H_2O was hydrothermally treated in a stainless steel Teflon-lined autoclave at 100 °C for 24 h. The obtained product

was continuously washed with distilled water and dried at room temperature. The surfactant was removed by calcination at 550 °C for 6 h in an air flow at a heating rate of 1 °C min^{-1} [16].

2.2. Synthesis of titania/silica materials

2.2.1. Synthesis of MTi/KIL-2 and MTi/SBA-15 using Ti-isopropoxide

The MTi/KIL-2(x) and MTi/SBA-15(x) powders were prepared by using Ti-isopropoxide (Ti(O^{i}Pr)$_4$) as a precursor and SBA-15 or KIL-2 synthesized support using acid-catalyzed sol–gel method which was described by Busuioc et al. [15]. Ti-isopropoxide was added gradually to aqueous solution of 1 M nitric acid (HNO_3) under continuous stirring for 2 h. Subsequently, the colloidal solution was diluted with deionized water and the pH was adjusted to 3 with 1 M sodium hydroxide (NaOH) solution. The pH adjustment was made to prevent destruction of the support by reaction with the acid. Then an appropriate amount of SBA-15 or KIL-2 was added to the colloidal dispersion. The mixture was stirred for 2 h at room temperature, followed by centrifugation and washing with deionized water, until the pH was about 6. The capillary force was believed to drive titania dispersion into the highly ordered mesoporous silica support. The solid product was dried at 60 °C and then calcined at 300 °C for 6 h. These samples were denoted as MTi/KIL-2(x) or MTi/SBA-15(x) where x is the molar ratio of Ti/Si that was adjusted to 1/1.

2.2.2. Synthesis of STi/KIL-2 and STi/SBA-15 using aqueous titania sol

The STi/KIL-2(x) and STi/SBA-15(x) powders were prepared using freshly made aqueous crystalline anatase-TiO_2 sol where $HClO_4$ as a peptizing agent and [Ti]/[H$^+$] ratio 2.5 was used [30]. The sol was deposited to the appropriate amount of SBA-15 or KIL-2 by the impregnation method. Before impregnation of sol to the support, the pH of the sol was adjusted to 3 with 1 M NaOH solution, resulting in a milky colloidal suspension. Here the pH adjustment was also made to prevent destruction of the support by reaction with the acid. Then a nominal amount of support was added to the colloidal dispersion. The mixture was stirred for 2 h at room temperature, followed by centrifugation and washing with deionized water, until the pH was about 6. The white precipitate was dried at 60 °C for 24 h. The samples prepared from KIL-2 and SBA-15 were designated as STi/KIL-2(x) and STi/SBA-15(x), respectively, where x is the molar ratio of Ti/Si that was adjusted to 1/2, 1/1 and 2/1.

The reference titania sample without silica support, i.e. the home-prepared specimen of low-temperature TiO_2 powder was obtained from the aqueous nanocrystalline anatase-TiO_2 sol (the same one as used for preparation of STi samples prior pH adjustment) by evaporation of solvent (water) at 50 °C for 12 h and drying in air at 150 °C for 3 h [30]. This sample was denoted as LT-TiO_2.

2.3. Characterization

The X-ray powder diffraction (XRD) patterns were obtained on a PANalytical X'Pert PRO high-resolution diffractometer with alpha 1 configuration using Cu$K_{\alpha 1}$ radiation (1.5406 Å) in the range from 0.5° to 5° for small-angle range and 5° to 60° for wide-angle range 2θ with a step size of 0.033 using a fully opened X'Celerator detector.

Porosity and specific surface area were evaluated by analysis of nitrogen adsorption isotherms measured on a Micromeritics Tristar 3000 instrument. These isotherms were recorded at 77 K. The samples were outgassed at 473 K for 2 h in the port of the adsorption analyzer. The BET specific surface area [32] was calculated from adsorption data in the relative pressure range from 0.05 to 0.2. The total pore volume (V_t) was estimated on the basis of the amount adsorbed at a relative pressure of 0.96 [33]. The primary mesopore volume (V_{me}) and the external surface area (S_{ex}) were determined using the α_s-plot method [33,34] from the adsorption data in the range of the standard reduced adsorption from 1.7 to 2.5 for SBA-15 materials and from 2.1 to 3.0 for KIL-2 materials. In the α_s-plot calculations, a macroporous silica material LiChrospher Si-1000 (S_{BET} = 22.1 m^2 g^{-1}) was used as a reference adsorbent [35]. The pore size distributions (PSDs) were calculated from nitrogen adsorption data using an algorithm based on ideas of Barrett, Joyner, and Halenda (BJH) [36]. The maximum on the PSD is considered as the primary mesopore diameter for given samples.

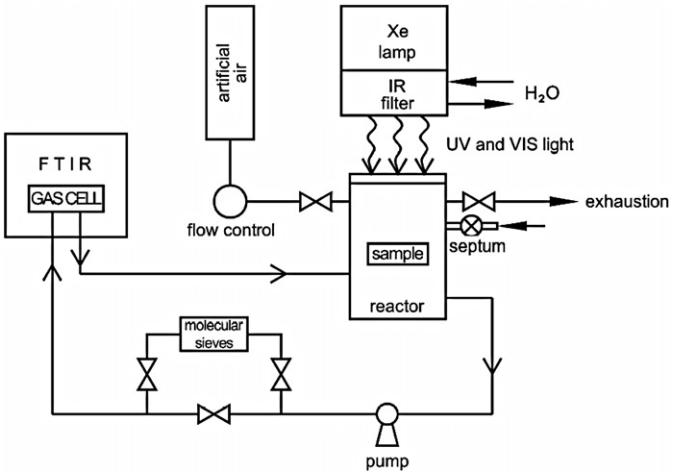

Fig. 1. The schematic diagram of the photocatalytic experimental set-up.

Morphology of samples was studied by scanning electron microscopy (SEM) on a Zeiss Supra^{TM} 3VP SEM microscope. Diffuse reflectance electronic spectra were measured using UV–vis–NIR spectrophotometer Lambda 19 (Perkin-Elmer) equipped with an integrating sphere. Powder samples were loaded in a 1 mm quartz cell and spectra were collected in the wavelength range from 200 to 800 nm.

2.4. Photocatalytic test

Photocatalytic activity of the powders presented in this work was evaluated by monitoring the degradation of a model organic compound in a gas medium with FT-IR spectroscopy. The model organic compound isopropanol was used which, upon irradiation, oxidizes into acetone and then into several further degradation products. A schematic diagram of the experimental set-up is shown in Fig. 1. A cylindrical reactor (1.4 L in volume) covered by quartz glass was constructed and connected by Teflon tubes to the FT-IR spectrometer. The whole system was hermetically sealed. The light source was a 300 W Xe lamp (Newport Oriel Instrument, USA). The infrared part of the spectrum was blocked by means of an adequate filter. The samples were prepared in the shape of a thin layer of powder with constant mass (50 mg) – and thus more or less constant thickness – in a Petri dish with 6 cm in diameter. The working distance between the Petri dish and the Xe lamp was 6 cm. Such an arrangement resulted in a light intensity of ~30 W m^{-2} in the UV range. Due to a strong influence of relative humidity on photocatalytic activity [37,38], the relative humidity at 23 °C in the system prior to the experiment was kept within the range of 25–30%. It was maintained by means of a flow of air passing through the molecular sieves until a pre-defined humidity was attained. Temperature and relative humidity were measured by thermo- and hydro-meter, respectively, which were placed into the reactor. Each experiment was performed by injecting 5 μL of liquid isopropanol (~1100 ppm in a gas phase) into the reacting system through a septum. The

total reaction time was set at 20 h. The lamp was turned on after a certain period of time to allow for equilibration of the adsorption of isopropanol onto the powder. The isopropanol degradation and acetone formation/degradation processes were followed by monitoring the calculated area of their characteristic peaks at 951 and 1207 cm^{-1}, respectively, in the IR spectra measured by a FT-IR spectrometer (Perkin-Elmer Spectrum BX, USA). The photocatalytic activity of the samples was evaluated as the rate constant of the initial acetone formation. At room temperature the photocatalytic oxidation of isopropanol to acetone is fast, whereas the subsequent oxidation of acetone to CO_2 and H_2O is slower [39]. At very short times the slope is proportional to the formation rate constant [40]. In addition, being the first intermediate of isopropanol degradation [41], the formation of acetone is a process that can easily be distinguished from the subsequent degradation process occurring during isopropanol photo-oxidation. A kinetic model was constructed to fit the experimental data in the range of acetone formation, enabling the calculation of acetone formation rate constants.

3. Results and discussion

3.1. The characterization of mesoporous solids

3.1.1. XRD analysis

The maintenance of the support framework order upon impregnation of titania and the effect of increasing the molar ratio was studied by the analysis of the small-angle range XRD patterns. The small-angle X-ray powder diffraction patterns in the range of $0.5^\circ < 2\theta < 5^\circ$ are illustrated in Fig. 2(I) and (II). In Fig. 2(I) the SBA-15 diffractogram illustrates three diffraction peaks corresponding to the (1 0 0), (1 1 0) and (2 0 0) reflections typical for 2D-hexagonal pore arrangement with *p*6mm symmetry. However, it can be seen in Fig. 2(I) that after loading of titania on SBA-15 in samples STi/SBA-15(*x*), the diffraction peaks are still present and their 2θ values are only slightly shifted, indicating that the channels with good order are maintained during preparation procedure; though, the intensity of peaks is decreased by increasing the Ti/Si molar ratio and in the STi/SBA-15(2/1) it becomes low. It is believed that the presence of titania could lead to random collapse of the mesoporous channels [15]. The most intense (1 0 0) diffraction peak was used to calculate the unit cell dimensions [24,27,29], which are reported in Table 1. The titania loading influences d_{100} and the unit cell dimensions for the STi/SBA-15(*x*) samples. However, the near retention of unit cell dimensions indicates that the structure of SBA-15 is maintained during the loading of titania, confirming that the hexagonal SBA-15 is stable [25,27]. For the sample MTi/SBA-15(1/1), as it is shown in Fig. 2(I), introduction of hydrolyzed Ti-isopropoxide strongly reduced the intensity of the low-angle diffraction peaks. Thus it can be assumed that this synthetic approach, which started from Ti-isopropoxide as a precursor and required an additional calcination step, was more detrimental to the silica framework structure [15,25]. This

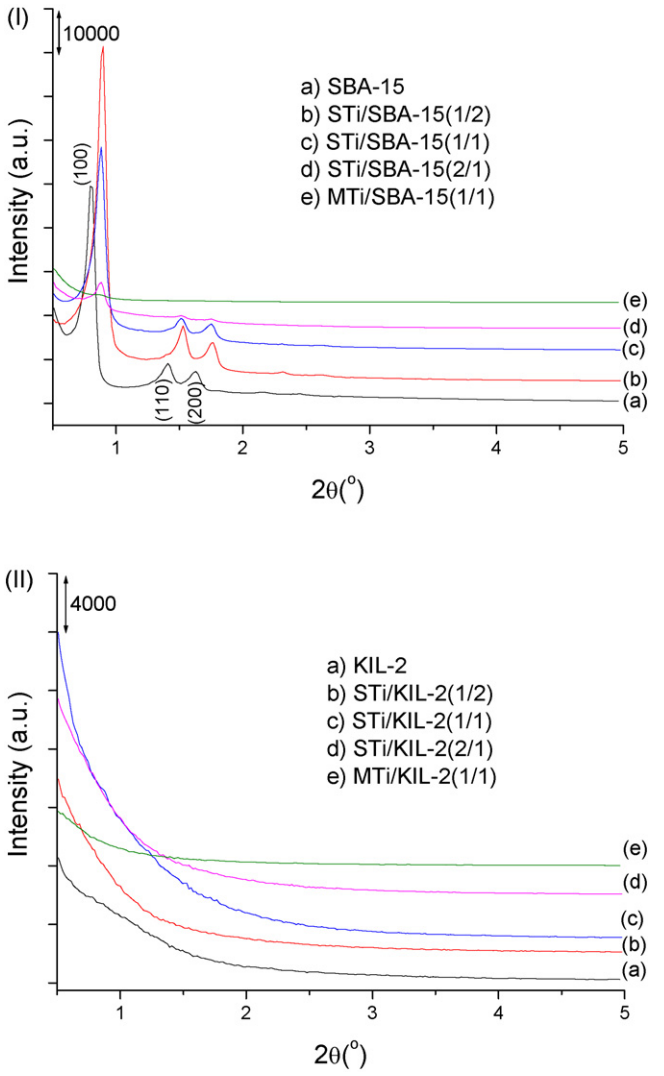

Fig. 2. Small-angle X-ray powder diffraction (XRD) patterns: (I) SBA-15, STi/SBA-15(*x*), MTi/SBA-15(1/1); (II) KIL-2, STi/KIL-2(*x*), MTi/KIL-2(1/1).

statement was also confirmed by SEM as it is shown below. The low-angle XRD patterns of KIL-2, MTi/KIL-2(1/1) and STi/KIL-2(*x*), as shown in Fig. 2(II), do not exhibit any peaks, indicating that the KIL-2 materials had a disordered mesoporous structure [31].

The X-ray diffractograms recorded in the wide-angle range ($5^\circ < 2\theta < 60^\circ$) are displayed in Fig. 3(I) and (II). They confirm that in both types of mesoporous silica materials, SBA-15 and KIL-2, anatase is the major crystalline phase in all prepared samples, as indicated by the peaks emerging at $2\theta = 25.3^\circ$, 37.8°, 48.1°, 53.9°, 55.1° associated with (1 0 1), (0 0 4), (2 0 0), (1 0 5), (2 1 1) anatase

Table 1
Structural parameters of powders determined from XRD and DRS.

Sample	Ti/Si molar ratio	Anatase crystallite size (nm)	d_{100} (Å)	Unit cell (nm)	Wall thickness (nm)	Band gap (eV)
SBA-15	–	–	111	12.73	7.73	–
STi/SBA-15(1/2)	1/2	–	98	11.28	4.28	3.39
STi/SBA-15(1/1)	1/1	–	100	11.52	6.52	3.20
STi/SBA-15(2/1)	2/1	12	100	11.52	6.52	3.14
MTi/SBA-15(1/1)	1/1	23	–	–	–	3.07
KIL-2	–	–	–	–	–	–
STi/KIL-2(1/2)	1/2	–	–	–	–	3.26
STi/KIL-2(1/1)	1/1	5	–	–	–	3.17
STi/KIL-2(2/1)	2/1	7	–	–	–	3.15
MTi/KIL-2(1/1)	1/1	19	–	–	–	3.04
LT–TiO_2	–	8	–	–	–	3.11

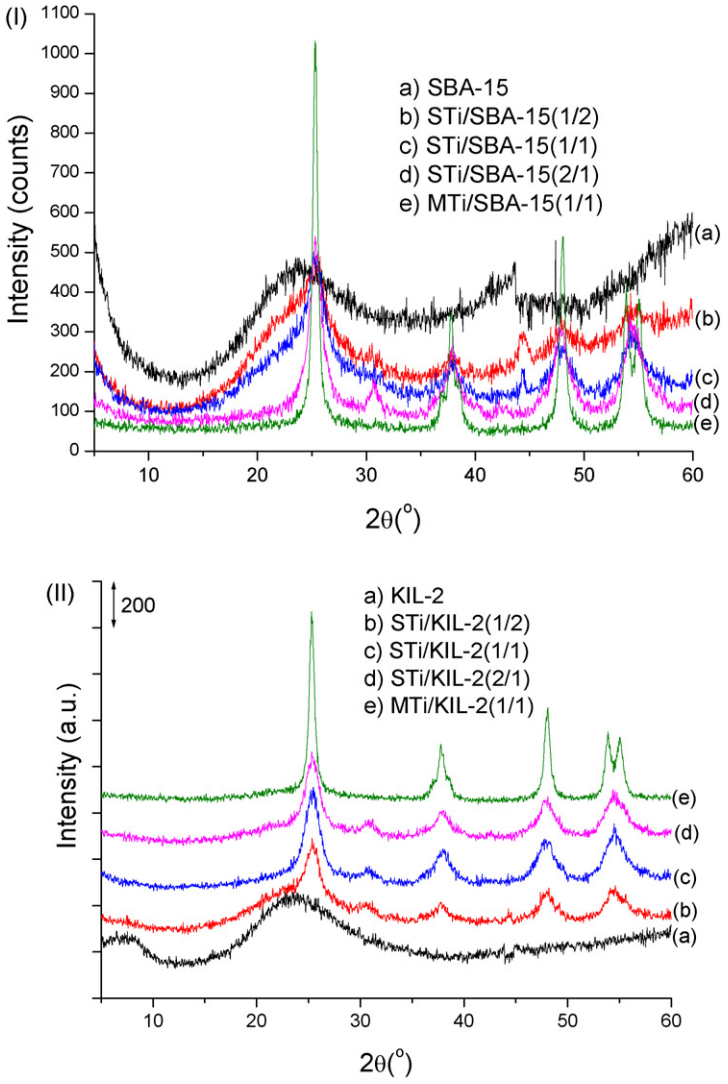

Fig. 3. Wide-angle X-ray powder diffraction (XRD): (I) SBA-15, STi/SBA-15(*x*), MTi/SBA-15(1/1); (II) KIL-2, STi/KIL-2 (*x*), MTi/KIL-2(1/1).

diffractions, respectively. The wide-angle XRD spectra of SBA-15 and KIL-2 possess one broad peak at 2θ around 23° corresponding to glass-like amorphous silicate nanoparticles while the crystalline titania phase is growing gradually by incorporation of titania. As can be seen in Fig. 3(I) and (II), the intensity of peaks is increased by increasing the Ti/Si molar ratio. It is important to mention that there is no difference in the position of the anatase peaks between the LT-TiO_2 sample (shown in our previous paper [30]) and silica-titania composites. In addition, by increasing the amount of titania, the presence of a brookite phase with a small peak at $2\theta = 30.8°$ becomes evident [42]. For the MTi/SBA-15(1/1) and MTi/KIL-2(1/1) powders, the anatase peaks are the strongest and sharpest compared to the other prepared samples which is a consequence of the different preparation procedure. In this case the grafting and growth of crystalline titania is obviously less disturbed by the host sites and additionally it forces the SBA-15 meso-ordered structure to collapse or it blocks the mesopores to such an extent that the low-angle diffraction peaks no longer appear (Fig. 2(I)). It is worthwhile mentioning that we did X-ray measurements for the STi/SBA-15(1/1) and STi/KIL-2(1/1) samples after calcination at 300 °C for 6 h as well. There was no significant difference noted between non-calcined and calcined samples.

The average crystallite sizes were determined from the Scherrer's equation using the broadening of the (1 0 1) anatase peak reflection with the usual assumption of spherical crystallites. We did not calculate the crystallite size of anatase in the samples with lower titania loading (STi/SBA-15(1/2), STi/SBA-15(1/1) and STi/KIL-2(1/2)) because there the anatase (1 0 1) peak interferes with the broad silica peak, making the determination of the half-height peak width difficult. As expected, the anatase nanocrystallites are much bigger in case of MTi/SBA-15(1/1) and MTi/KIL-2(1/1) samples, confirming that the titania source (pre-crystallized colloidal solution or hydrolyzed Ti-isopropoxide solution) has an important effect on the structure of silica-titania composites.

The band-gap energies determined for all the synthesized powders are reported in Table 1. The band-gap energy of LT-TiO_2, where the growth of anatase crystallites is unperturbed, is 3.11 eV. However, it changes when impregnated within silica support. By increasing the Ti/Si molar ratio from 1/2 to 2/1, the band-gap energy decreases from 3.39 to 3.14 eV in STi/SBA-15(*x*) and from 3.26 to 3.15 eV in STi/KIL-2(*x*) samples. These results are correlated with the crystalline size of the anatase, being smaller at lower loadings due to their fit in the open pores of the silica support and formation of plugged mesopores, where anatase nanocrystallites with a limited size can be accommodated. By increasing the particle size, the band-gap energy decreases. The band-gap energies of MTi/SBA-15(1/1) and MTi/KIL-2(1/1) are 3.07 and 3.04 eV, respectively, resembling the values characteristic of LT-TiO_2.

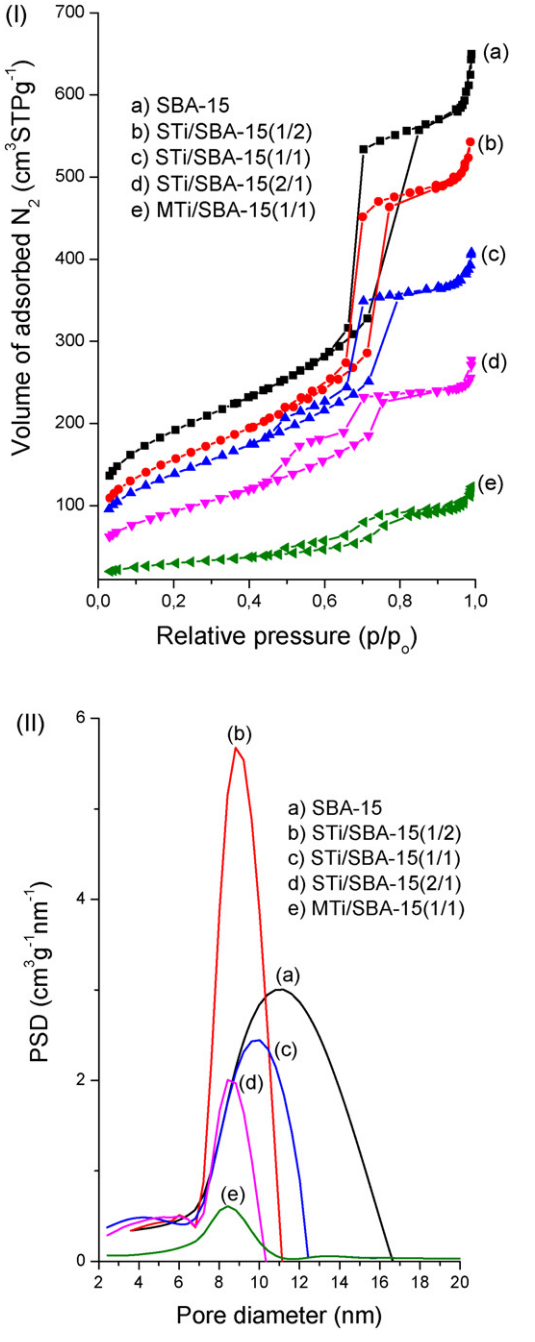

Fig. 4. (I) The nitrogen adsorption isotherms; (II) pore size distribution of SBA-15, STi/SBA-15(x), MTi/SBA-15(1/1).

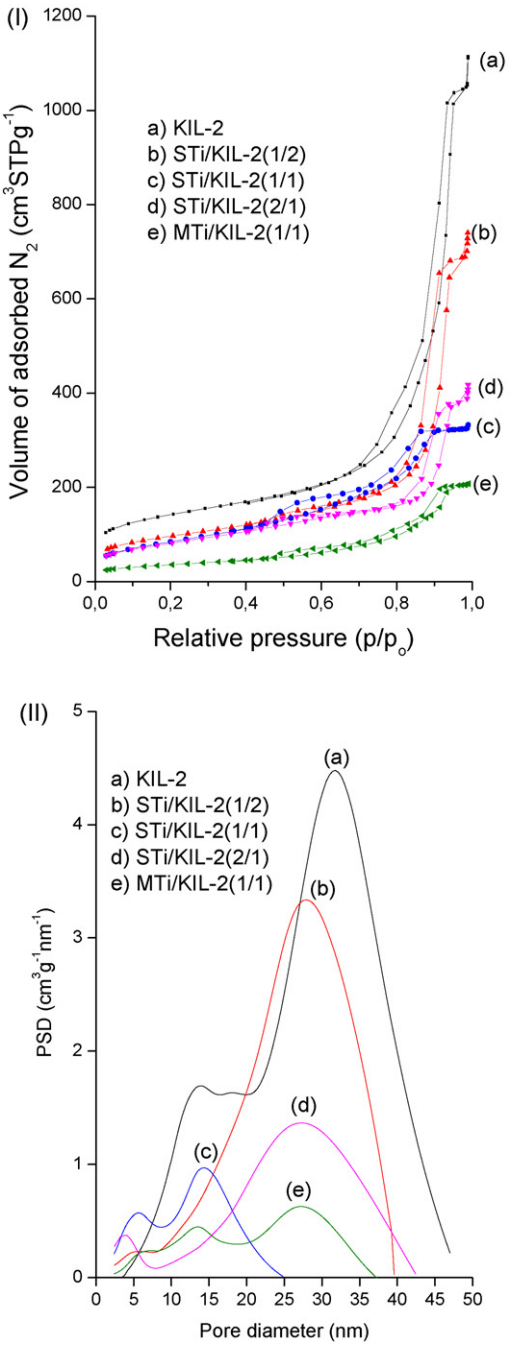

Fig. 5. (I) The nitrogen adsorption isotherms; (II) pore size distribution of KIL-2, STi/KIL-2(x), MTi/KIL-2(1/1).

3.1.2. N_2 sorption measurements

Nitrogen adsorption isotherms for SBA-15, MTi/SBA-15(1/1) and STi/SBA-15(x) powders are shown in Fig. 4(I), whereas structural parameters determined on the basis of these isotherms are listed in Table 2. SBA-15 sample exhibited adsorption isotherm typical for SBA-15 silica, that is, with relatively narrow hysteresis loop of H1 type [33]. It can clearly be observed that the presence of TiO_2 in SBA-15 leads to a marked change in the shape of the hysteresis loop. The hysteresis loop of all samples is closing down at lower relative pressure values in comparison to the original support (SBA-15), which indicates that the pores are partially narrowed with titania nanoparticles. The increase of the amount of the deposited TiO_2 nanoparticles on SBA-15 prepared by aqueous TiO_2 sol not only led to a decrease of specific surface area (from 589 to 336 $m^2\ g^{-1}$), total pore volume (from 0.903 to 0.378 $cm^3\ g^{-1}$), primary mesopore volume (from 0.682 to 0.303 $cm^3\ g^{-1}$), and pore diameter (from 11.2 to 8.6 nm) but also resulted in an appreciable widening and tailing of hysteresis loops and in a two-step desorption, thus evidencing the formation of PHTS-like material [13,43,44]. N_2 sorption isotherms of PHTS are of type IV according to the IUPAC classification [33], showing a one-step capillary condensation, indicating the filling of the uniform mesopores and two-step desorption. The first step is similar with desorption in pure SBA-15 and is assigned to desorption of N_2 from the open pores; the second desorption step can be attributed to the nanoparticles (plugs) within the mesopores (the narrowed mesopores) [10,11]. The second step on the desorption branch indicates the existence of plugged mesopores. This two-step desorption is similar to that of the PHTS materials with

Table 2
Structural parameters of powders determined from N_2 sorption measurements.

Sample	S_{BET} ($m^2\ g^{-1}$)	V_t ($cm^3\ g^{-1}$)	V_{me} ($cm^3\ g^{-1}$)	S_{ex} ($m^2\ g^{-1}$)	S_{me} ($m^2\ g^{-1}$)	$w_{BJH}(1)$ (nm)	$w_{BJH}(2)$ (nm)
SBA-15	589	0.903	0.682	114	488	11.2	–
STi/SBA-15(1/2)	560	0.779	0.580	87	447	8.9	6.0
STi/SBA-15(1/1)	498	0.578	0.491	58	410	9.3	4.2
STi/SBA-15(2/1)	336	0.378	0.303	51	310	8.6	5.2
MTi/SBA-15(1/1)	107	0.154	0.097	37	90	8.4	–
KIL-2	504	1.561	1.337	122	324	31.6	13.718.2
STi/KIL-2(1/2)	345	1.016	0.728	157	278	27.9	5.5
STi/KIL-2(1/1)	309	0.499	0.488	8	322	14.2	5.5
STi/KIL-2(2/1)	296	0.577	0.501	52	287	27.4	3.8
MTi/KIL-2(1/1)	130	0.306	0.303	9	115	27.4	6.613.7
LT-TiO_2	80	–	–	–	–	–	–

S_{BET}: the BET surface area; V_t: total pore volume evaluated from adsorption isotherm at the relative pressure about 0.96; V_{me}: primary mesopore volume evaluated by the α_s-method; S_{ex}: external surface area evaluated by α_s-method; S_{me}: mesoporous surface area evaluated by α_s-method; w_{BJH}: mesopore diameters at the maximum (maxima) of the BJH pore size distribution.

amorphous microporous silica nanoparticles (plugs) in the mesopores [11,16,43]. It can be concluded that the titania nanoparticles have been dispersed inside the channels of SBA-15 thereby narrowing parts of the mesopores. Therefore, desorption is postponed to lower relative pressures resulting in the second desorption step. Further increase of the titania amount results in a more pronounced growth of the titania nanoparticles causing a significant decrease of the open pores volume and in the change of the second desorption step. When titania loading is further increased the growth of the titania particles on the external surface is expected. The decrease of the interparticle (textural) porosity (given by the small hysteresis at $P/P_0 = 0.95–1$) suggests the growth of the TiO_2 nanoparticles on the outer surface, filling the voids between SBA-15 particles. The shape of isotherms of samples STi/SBA-15(1/1) and MTi/SBA-15(1/1) (Fig. 4(I)) are different due to a different precursor. The primary mesopore volume and pore diameter of MTi/SBA-15(1/1) are significantly lower than for STi/SBA-15(1/1). The preparation method using Ti-isopropoxide as titania source also caused the destruction of ordered mesostructure, which is in agreement with the XRD pattern of this material.

Pore size distribution of the different mesoporous materials has been determined using the BJH model widely used for these types of sample [45]. Although this model often underestimates pore sizes [46], it is appropriate for comparative purposes. The Fig. 4(II) displays the pore size distribution determined from adsorption isotherms. It is clear that after impregnation two maxima appear representing the open mesopores located at the mesopore mouths and the narrowed pores in which the pore radius has shifted to lower values [15], while pore size distribution of pure SBA-15 shows only one maximum. As it can be observed, the maxima characteristic to open mesopores shift to lower pore sizes [28], are less intense and become broader with the growth of the titania plugs located inside the channels. At the same time, the maxima characteristic for narrowed pores shift to lower pore size values and are broader. Impregnating higher amounts of titania results in a lower amount of open pores present in the material. These results match with previous observations, where the pore size distribution shifted to lower pore diameters [28]. The difference between two types of precursor is also evidenced from the pore size distribution of MTi/SBA-15(1/1) sample, where only one broad maximum appears.

Nitrogen adsorption isotherms for KIL-2, MTi/KIL-2(1/1) and STi/KIL-2(x) powders are shown in Fig. 5(I), whereas structural parameters determined on the basis of these isotherms are listed in Table 2. KIL-2 sample exhibited an adsorption isotherm typical for KIL-2 silicas [31], that is, with relatively narrow hysteresis loop of type IV [33]. It can be clearly observed that the introduction of titania into KIL-2 also leads to a marked change in the shape of the hysteresis loop. Again, the hysteresis loop of all samples is closing down at lower P/P_0 values in comparison to the original support, which indicates that the pores are partially narrowed with titania nanoparticles. The increase of the amount of the deposited titania nanoparticle on KIL-2 led to a decreased specific surface area (from 504 to 296 $m^2\ g^{-1}$), total pore volume (from 1.561 to 0.499 $cm^3\ g^{-1}$), primary mesopore volume (from 1.337 to 0.488 $cm^3\ g^{-1}$), and pore diameter (from 31.6 to 14.2 nm). Besides these changes an appreciable widening and tailing of hysteresis loops and/or a two-step desorption were observed, thus evidencing the formation of materials with plugs in pores. The first step is similar with desorption in pure KIL-2 and is assigned to the desorption of N_2 from the open pores; the second desorption step can be attributed to the nanoparticles (plugs) within the mesopores (the narrowed mesopores) [10,11]. A second step on the desorption branch indicates the existence of plugged mesopores. Therefore, it can be concluded that the titania nanoparticles have been dispersed inside the pores of KIL-2 thereby narrowing parts of the mesopores. Further increase of the titania amount results in a significant decrease of the open pore volumes and in the change of the second desorption step. Higher titania loadings caused the growth of titania particles on the external surface. This evidence is clearly seen in a relative pressure range from 0.95 to 1, where hysteresis loops due to textural porosity become smaller. The pore size distribution determined from adsorption isotherms of KIL-2 shows 3 distinguished maxima (Fig. 5(II)). Pore size distributions of STi/KIL-2(x) samples show only 2 maxima, while pore size distribution of MTi/KIL-2(1/1) sample shows 3 maxima. As it can be observed, the maxima characteristic to open mesopores and to narrowed pores shift to lower pore sizes, are less intense and become broader with the growth of the titania plugs located inside the channels.

3.1.3. Scanning electron microscopy

The SEM micrographs of all the various samples are shown in Figs. 6 and 7. The SEM image of pure SBA-15 presented in Fig. 6(a) shows curved rod-like particles of relatively uniform size with a quite smooth surface [16]. In the STi/SBA-15(1/2) and STi/SBA-15(1/1) samples, as evidenced from Fig. 6(b) and (c), these powders show a homogenous distribution of the titania on the internal surface of SBA-15 powder and the morphology of samples does not change compared to pure SBA-15. However, at higher titania loading in the STi/SBA-15(2/1) sample, the external surface of SBA-15 is filled significantly by titania (Fig. 6(d)), which is in accordance with the N_2 sorption results. In the MTi/SBA-15(1/1) sample (Fig. 6(e)), impregnation of hydrolyzed Ti-isopropoxide changed the morphology of SBA-15 drastically, again well in accordance with the results discussed above.

As it is shown in Fig. 7(a), the SEM micrograph of KIL-2 powder is characterized by the porous and rough surface. In fact these powders suggest the main type of porosity, which is so-called inter-

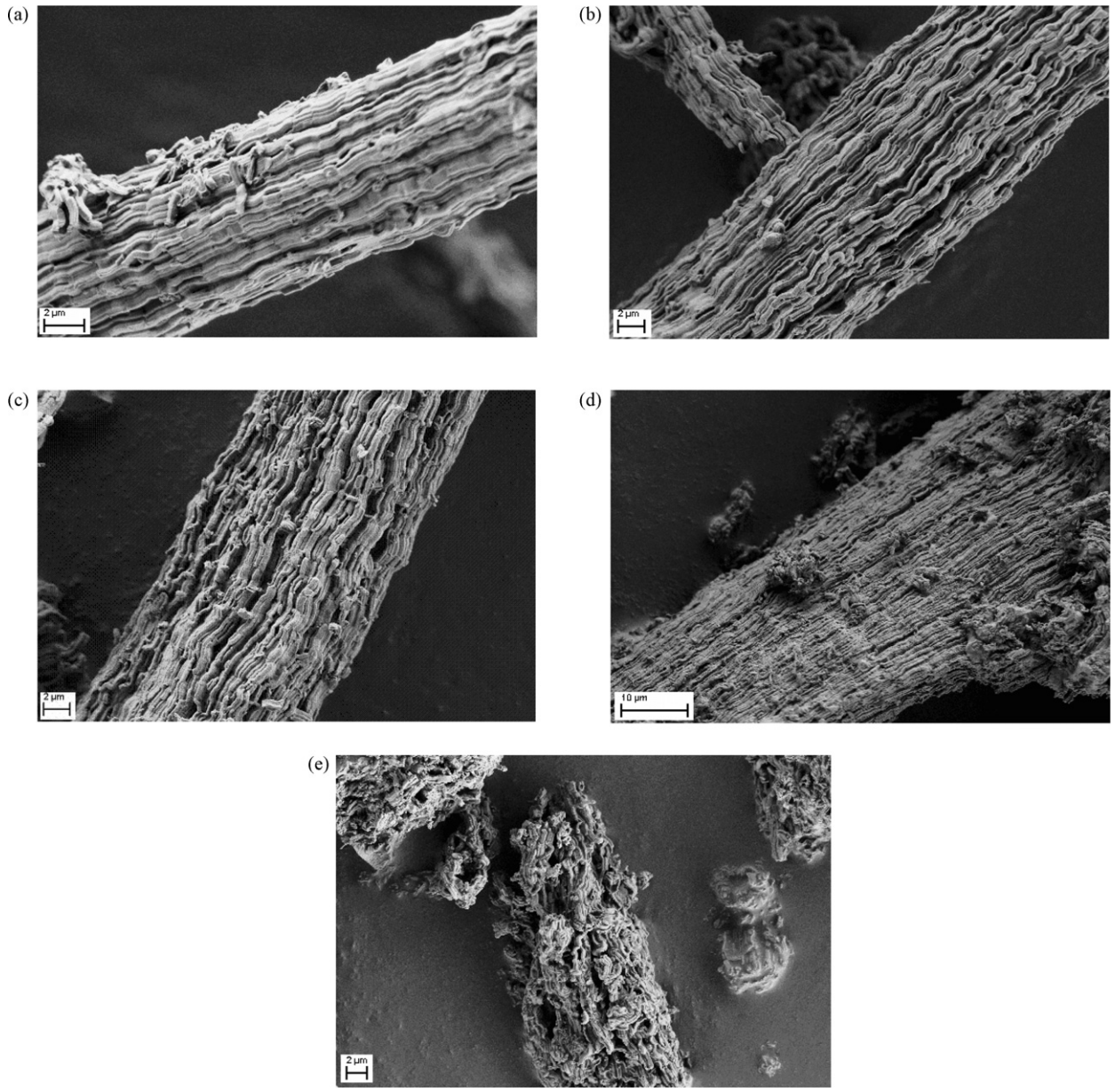

Fig. 6. SEM images of (a) SBA-15, (b) STi/SBA-15(1/2), (c) STi/SBA-15(1/1), (d) STi/SBA-15(2/1) and (e) MTi/SBA-15(1/1).

particle or textural porosity [31]. The roughness in the surface of KIL-2 increases by adding titania. Thus by increasing the Ti/Si molar ratio from 1/2 to 2/1 in the STi/KIL-2(x) samples, the roughness increases considerably (Fig. 7(b)–(d)). In the MTi/KIL-2(1/1) sample, as it is represented in Fig. 7(e), the roughness of KIL-2 seems to decrease resulting in a less textured surface.

3.2. The photocatalytic activity testing

Figs. 8 and 9 illustrate the adsorption capacity and the formation of acetone during the photocatalytic degradation of isopropanol in the presence of different samples. Additionally, the profiles of acetone and isopropanol in the absence of a photocatalyst (blank) were included in the graphs. In all tests at the beginning of the experiment the UV lamp was switched off to achieve an adsorption–desorption equilibrium. The adsorption–desorption equilibrium times were not the same for various samples. Some adsorption took place also in the absence of a photocatalyst sample (onto the surfaces of the reactor system). In Figs. 8(I) and 9(I) the time zero represents the point when the UV lamp was switched on. Before that, there was no detectable degradation of isopropanol in the dark but nevertheless the isopropanol concentration decreased, mostly due to the adsorption of isopropanol on the catalyst powders. In the case of SBA-15, MTi/SBA-15(1/1) and STi/SBA-15(x) (Fig. 8(I)) the adsorption capacity of SBA-15 was the highest which corresponds to the highest surface area of SBA-15 powders. By loading with titania, the adsorption capacity of the samples decreased, roughly in accordance with the decreasing specific surface area (Table 2). For example, the surface area decreased from 560 to 336 $m^2\,g^{-1}$ for STi/SBA-15(1/2) and STi/SBA-15(2/1), respectively. The adsorption capacity of the home-prepared specimen (LT-TiO_2) is very low which is not surprising due to its relatively low surface area (80 $m^2\,g^{-1}$). The photocatalytic activity of the powders was assessed according to the value of the rate constant (k_1) representing the oxidation of isopropanol into acetone. The analysis of data was based on the following two-step oxidation mechanism:

$$\text{isopropanol} \xrightarrow{k_1} \text{acetone} \xrightarrow{k_2} \text{further oxidation products} \quad (1)$$

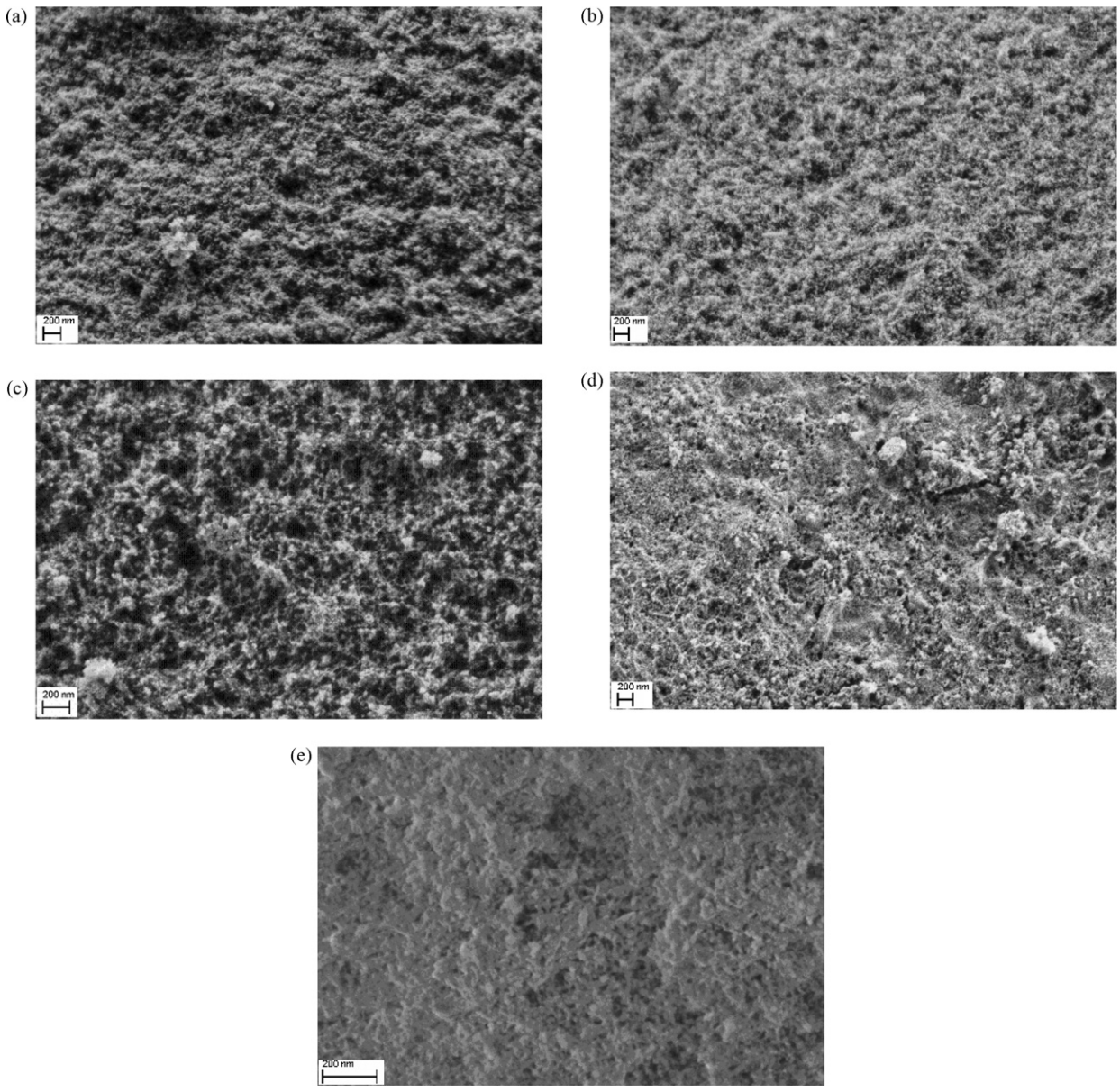

Fig. 7. SEM images of (a) KIL-2, (b) STi/KIL-2(1/2), (c) STi/KIL-2(1/1), (d) STi/KIL-2(2/1) and (e) MTi/KIL-2(1/1).

where k_1 and k_2 are the corresponding rate constants. As regards the order of these two steps, the first step is usually considered a zero-order reaction [47,48] while the second step can be assumed to be a first-order reaction. These assumptions lead to the following equation for the concentration of acetone as a function of time ($C_{acet}(t)$):

$$C_{acet}(t)(\text{zero}) = \frac{k_1}{k_2}(1 - e^{-k_2 t}) \quad (2)$$

According to this simplified model, at the time t (peak) all isopropanol has been consumed and the acetone curve exhibits a peak (maximum concentration). However, it has been shown that the interpretation of the appearance of peak might be much more complex than indicated by Eqs. (1) and (2). Besides being created due to the exhaustion of the supply of isopropanol vapour to the irradiated titania surface, one needs to take into account the re-adsorption of the acetone vapour upon the titania. In fact, the process of acetone re-adsorption might even be a decisive step, especially because the degradation rate of acetone might be relatively slow. In any case, the initial slope of the curve is independent of these further complications, so the data obtained from this initial slope are usually quite reliable. In our case, we use these data mainly for rough comparison of different catalysts without attempting to find exact absolute values for rate constants or exact underlying mechanisms. The trends in k_1 for different catalysts prepared in this study are seen from Table 3.

As expected, SBA-15 did not show any photocatalytic activity. However, the photocatalytic activity of STi/SBA-15(x) increased by increasing the Ti/Si ratio from 1/2 to 1/1 (STi/SBA-15(1/2) and STi/SBA-15(1/1)), but in STi/SBA-15(2/1) it decreased significantly. As shown in XRD results, the crystallinity and the number of anatase nanoparticles increased when the Ti/Si molar ratio was raised from 1/2 to 1/1 resulting in the high photocatalytic activity. However, by increasing the Ti/Si molar ratio further to 2/1 in the STi/SBA-15(2/1) sample, the partial blocking of mesopores occurred and the external surface of SBA-15 began to fill with the high amount of titania, as it is demonstrated above from N_2 sorption and SEM results. Therefore, the photocatalytic activity was the highest in the presence of the STi/SBA-15(1/1) powders. In MTi/SBA-15(1/1) sample, having the same nominal Ti/Si molar ratio as STi/SBA-15(1/1), the adsorption

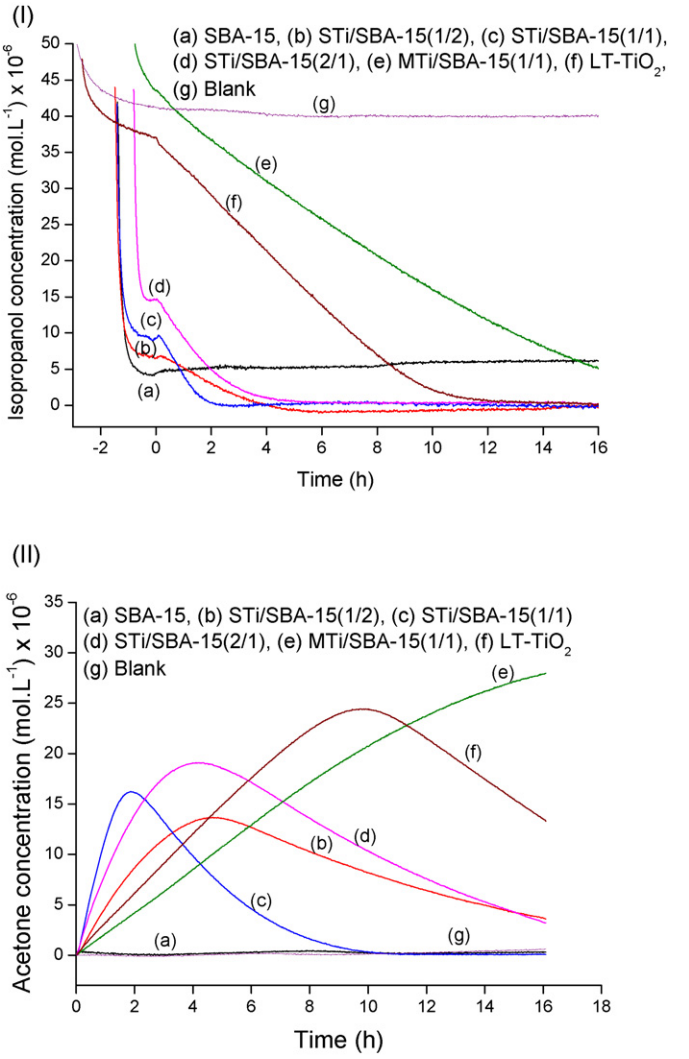

Fig. 8. (I) Dark adsorption of isopropanol (negative illumination times) and its photocatalytic disappearance; (II) acetone formation curves in presence of SBA-15, STi/SBA-15(x), MTi/SBA-15(1/1), home-prepared specimen low-temperature TiO_2 (LT-TiO_2), blank.

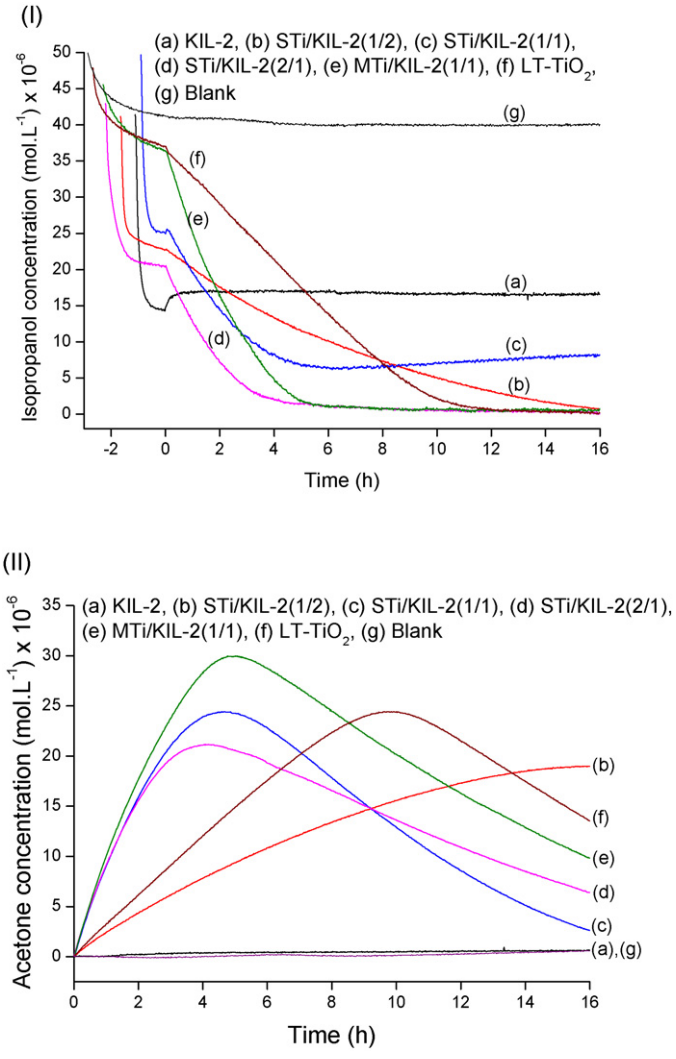

Fig. 9. (I) Dark adsorption of isopropanol (negative illumination times) and its photocatalytic disappearance; (II) acetone formation curves in presence of KIL-2, STi/KIL-2(x), MTi/KIL(1/1), home-prepared specimen low-temperature TiO_2 (LT-TiO_2), blank.

capacity and photocatalytic activity were very low. It is reported in Table 2 that the MTi/SBA-15(1/1) sample has the lowest surface area compared to other supported samples, whereas it has the most developed anatase crystalline structure (Fig. 3(I)). As shown by XRD and SEM results, the structure of SBA-15 support was completely destroyed by using Ti-isopropoxide as a titania precursor. It should be pointed out that the high crystallinity in MTi/SBA-15(1/1) sample is also due to the calcination treatment at 300 °C for 6 h during the synthesis procedure.

Table 3
The acetone formation rate in the presence of different powders.

Sample	Acetone formation rate constant, k_1 ($\times 10^{-5}$ mol L^{-1} h^{-1})
SBA-15	–
STi/SBA-15(1/2)	1.07
STi/SBA-15(1/1)	2.68
STi/SBA-15(2/1)	1.19
MTi/SBA-15(1/1)	0.25
KIL-2	–
STi/KIL-2(1/2)	0.32
STi/KIL-2(1/1)	1.06
STi/KIL-2(2/1)	1.20
MTi/KIL-2(1/1)	1.02
LT-TiO_2	0.50

Note: The values for k_1 were calculated from $k_1(\text{zero}) = C_0/t$ (peak). For all samples, the value of C_0 is taken as equal to the injected concentration, that is 5×10^{-5} mol L^{-1}.

In the case of KIL-2, MTi/KIL-2(1/1) and STi/KIL-2(x) (Fig. 9(I) and (II)) there are some important differences in comparison with samples using SBA-15 support. First, the adsorption capacity of KIL-2 was lower than SBA-15 due to its lower surface area in comparison to SBA-15 materials. The adsorption capacity of the STi/KIL-2(x) samples decreased as the Ti/Si ratio increased from 1/2 to 1/1 (samples STi/KIL-2(1/2) and STi/KIL-2(1/1)). However, it slightly increased for STi/KIL-2(2/1) even though its surface area was slightly lower than STi/KIL-2(1/1). This can be due to the interparticle or textural properties of KIL-2 materials. The acetone formation rate (Fig. 9(II)) increased significantly by increasing the amount of titania from STi/KIL-2(1/2) to STi/KIL-2(1/1), while at the highest titania loading, STi/KIL-2(2/1), it remained approximately the same. However, in the presence of the MTi/KIL-2(1/1) sample, the adsorption capacity was very low due to the low surface area but interestingly, the photocatalytic activity of this sample was comparable to the of STi/KIL-2(1/1) powder. Here, the structure of the support was not destroyed upon using the Ti-isopropoxide as a precursor (Fig. 7(e)), also the hysteresis loop in the N_2 sorption measurements is well evident (Fig. 5(I)).

Note that the samples that were prepared using SBA-15 as a support had a higher adsorption capacity. This can directly be explained by their higher surface area. Regarding the photocatalytic activity (acetone formation), when the Ti/Si molar ratio was 1/2 and 1/1, the samples which were prepared using SBA-15 showed higher photocatalytic activity. This means that the photocatalytic activity of STi/SBA-15(1/2) and STi/SBA-15(1/1) is higher than the photocatalytic activity of STi/KIL-2(1/2) and STi/KIL-2(1/1). But when the Ti/Si molar ratio was 2/1, the photocatalytic activity of the STi/KIL-2(2/1) sample was comparable to the activity of STi/SBA-15(2/1) (similar acetone formation rate constant). The acetone formation rate constants are summarized for all studied samples in Table 3. As it is reported, the acetone formation rate was the highest in the presence of the STi/SBA-15(1/1) sample, indicating the importance of maintaining high mesostructural order of the silica support upon titania loading and its influence of keeping the titania nanoparticles relatively separated and accessible.

4. Conclusions

Titania-containing ordered and disordered mesoporous silica (SBA-15 and KIL-2) have been synthesized with different Ti/Si molar ratios (1/2, 1/1, 2/1) using sol–gel impregnation method. Titanium isopropoxide in acidic solution and aqueous nanocrystalline titania sol were used as a source of titania. The properties of the prepared samples depend on titania precursor, preparation conditions and the type of the framework of the mesoporous silica materials. Ordered mesoporous SBA-15 type and disordered mesoporous KIL-2 type with textural porosity has a major effect on the structural properties and photocatalytic activity. The results demonstrate that the order of the SBA-15 framework was maintained upon impregnation of titania sol while it was destroyed by using Ti-isopropoxide. The increase of Ti/Si molar ratio led to decrease of the surface area and random dispersion of titania nanoparticles inside the channels of SBA-15 thus narrowing parts of the mesopores of SBA-15. Further increase of titania amount results on the growth of the titania particles on the external surface of the silica support. The adsorption capacities of the titania-containing SBA-15 powders are in concurrence with the surface area which is decreasing by increasing the titania amount (the growth of anatase plugs inside the channels of SBA-15 materials). Thus the total capacity to adsorb isopropanol is the highest in the presence of SBA-15, which is in agreement with the highest surface area of SBA-15 and decreases with the growth of the titania nanoparticles due to partial blocking of the mesopores. The adsorption capacities of titania-containing KIL-2 powders shows the behavior similar to the titania-containing SBA-15, with an exception of STi/KIL-2(2/1) powder, where the adsorption capacity was higher than expected. The photocatalytic activity towards formation of acetone depends on the accessibility and the number of titania nanoparticles. In the STi/SBA-15(1/1) sample, the loading of titania was not too high to decrease accessibility and not too low to ensure sufficient quantity of active nanoparticles for reaction, therefore among all the investigated samples the photocatalytic activity (acetone formation rate) of STi/SBA-15(1/1) was the highest. Our results confirm the beneficial influence of the mesoporous support on the low-temperature prepared titania for the removal of an organic contaminant from the gaseous phase, at the dark adsorption as well as at the photocatalytic stage of the process.

Acknowledgements

This research was supported by the Ministry of Higher Education, Science and Technology of the Republic of Slovenia. We would like to acknowledge Dr. Jaromir Jirkovsky from the J. Heyrovsky Institute of Physical Chemistry in Prague for measuring the diffuse reflectance spectra and determination of the band-gap energies.

References

[1] J.S. Kresge, M.E. Leonowicz, W.J. Roth, J.C. Vartuli, J.S. Beck, Ordered mesoporous molecular sieves synthesized by a liquid crystal template mechanism, Nature 359 (1992) 710–712.
[2] W.-H. Zhang, J.-L. Shi, H.-R. Chen, Z.-L. Hua, D.-S. Yan, Synthesis and characterization of nanosized ZnS confined in ordered mesoporous silica, Chem. Mater. 13 (2001) 648–654.
[3] D. Zhao, J. Feng, Q. Huo, N. Melosh, G.H. Fredrickson, B.F. Chmelka, G.D. Stucky, Triblock copolymer syntheses of mesoporous silica with periodic 50 to 300 angstrom pores, Science 279 (1998) 548–552.
[4] S. Inagaki, Y. Fukushima, K. Kuroda, Synthesis of highly ordered mesoporous materials from a layered polysilicate, J. Chem. Soc., Chem. Commun. (1993) 680–682.
[5] P.T. Tanev, T.J. Pinnavaia, A natural templating route to mesoporous molecular sieves, Science 267 (1995) 865–867.
[6] P.T. Tanev, M. Chibwe, T.J. Pinnavaia, Titanium-containing mesoporous molecular sieves for catalytic oxidation of aromatic compounds, Nature 368 (1994) 321–322.
[7] S.A. Bagshaw, E. Prouzet, T.J. Pinnavaia, Templating of mesoporous molecular sieves by nonionic polyethylene oxide surfactants, Science 269 (1995) 1242–1244.
[8] E. van Bavel, P. Cool, Morphology variations of plugged hexagonal templated silica, J. Porous Mater. 12 (2005) 65–69.
[9] E. van Bavel, P. Cool, K. Aerts, E.F. Vansant, Plugged hexagonal templated silica (PHTS): an in-depth study of the structural characteristics, J. Phys. Chem. B 108 (2004) 5263–5268.
[10] P. van der Voort, P.I. Ravikovitch, K.P. de Jong, M. Benjelloun, E. van Bavel, A.H. Janssen, A.V. Neimark, B.M. Weckhuysen, E.F. Vansant, A new templated ordered structure with combined micro- and mesopores and internal silica nanocapsules, J. Phys. Chem. B 106 (2002) 5873–5877.
[11] M. Kruk, M. Jaroniec, S.H. Joo, R. Ryoo, Characterization of regular and plugged SBA-15 silicas by using adsorption and inverse carbon replication and explanation of the plug formation mechanism, J. Phys. Chem. B 107 (2003) 2205–2213.
[12] P. van der Voort, P.I. Ravikovitch, K.P. de Jong, A.V. Neimark, A.H. Janssen, M. Benjelloun, E. van Bavel, P. Cool, B.M. Weckhuysen, E.F. Vansant, Plugged hexagonal templated silica: a unique micro- and mesoporous composite material with internal silica nanocapsules, Chem. Commun. (2002) 1010–1011.
[13] E.B. Celer, M. Kruk, Y. Zuzek, M. Jaroniec, Hydrothermal stability of SBA-15 and related ordered mesoporous silicas with plugged pores, J. Mater. Chem. 16 (2006) 2824–2833.
[14] K. Miyazawa, S. Inagaki, Control of the microprosity within the pore walls of ordered mesoporous silica SBA-15, Chem. Commun. (2000) 2121–2122.
[15] A.M. Busuioc, V. Meynen, E. Beyers, M. Mertens, P. Cool, N. Bilba, E.F. Vansant, Structural features and photocatalytic behaviour of titania deposited within the pores of SBA-15, Appl. Catal. A: General 312 (2006) 153–164.
[16] M. Mazaj, W.J.J. Stevens, N. Zabukovec Logar, A. Ristić, N. Novak Tušar, I. Arčon, N. Daneu, V. Meynen, P. Cool, E.F. Vansant, V. Kaučič, Synthesis and structural investigations on aluminium-free Ti-Beta/SBA-15 composite, Micropor. Mesopor. Mater. 117 (2009) 458–465.
[17] Z. Luan, E.M. Maes, P.A.W. van der Heide, D. Zhao, R.S. Czernuszewicz, L. Kevan, Incorporation of titanium into mesoporous silica molecular sieve SBA-15, Chem. Mater. 11 (1999) 3680–3686.
[18] Y. Segura, P. Cool, P. van der Voort, F. Mees, V. Meynen, E.F. Vansant, TiO_x–VO_x mixed oxides on SBA-15 support prepared by the designed dispersion of acetylacetonate complexes: spectroscopic study of the reaction mechanisms, J. Phys. Chem. B 108 (2004) 3794–3800.
[19] A. Fujishima, K. Hashimoto, T. Watanabe, TiO_2 Photocatalysis: Fundamentals and Applications, BKC, Inc., Tokyo, 1999.
[20] D. Sun, Z. Liu, J. He, B. Han, J. Zhang, Y. Huang, Surface sol–gel modification of mesoporous silica molecular sieve SBA-15 with TiO_2 in supercritical CO_2, Micropor. Mesopor. Mater. 80 (2005) 165–171.
[21] Z. Luan, L. Kevan, Characterization of titanium-containing mesoporous silica molecular sieve SBA-15 and generation of paramagnetic hole and electron centers, Micropor. Mesopor. Mater. 44–45 (2001) 337–344.
[22] S. Perathoner, P. Lanzafame, R. Passalacqua, G. Centi, R. Schlogl, D.S. Su, Use of mesoporous SBA-15 for nanostructuring titania for photocatalytic applications, Micropor. Mesopor. Mater. 90 (2006) 347–361.
[23] B.J. Aronson, C.F. Blanford, A. Stein, Solution-phase grafting of titanium dioxide onto the pore surface of mesoporous silicates: synthesis and structural characterization, Chem. Mater. 9 (1997) 2842–2851.
[24] G. Calleja, R. van Grieken, R. Garcia, J.A. Melero, J. Iglesias, Preparation of titanium molecular species supported on mesostructured silica by different grafting methods, J. Mol. Catal. A: Chem. 182–183 (2002) 215–225.
[25] R. van Grieken, J. Aguado, M.J. Lopez-Munoz, J. Marugan, Synthesis of size-controlled silica-supported TiO_2 photocatalysts, J. Photochem. Photobiol. A: Chem. 148 (2002) 315–322.
[26] M.-J. Lopez-Munoz, R. van Grieken, J. Aguado, J. Marugan, Role of the support on the activity of silica-supported TiO_2 photocatalysts: structure of the TiO_2/SBA-15 photocatalysts, Catal. Today 101 (2005) 307–314.

[27] H. Ding, H. Sun, Y. Shan, Preparation and characterization of mesoporous SBA-15 supported dye-sensitized TiO_2 photocatalyst, J. Photochem. Photobiol. A: Chem. 169 (2005) 101–107.
[28] M.V. Landau, L. Vradman, X. Wang, L. Titelman, High loading TiO_2 and ZrO_2 nanocrystals ensembles inside the mesopores of SBA-15: preparation, texture and stability, Micropor. Mesopor. Mater. 78 (2005) 117–129.
[29] W. Wang, M. Song, Multistep impregnation method for incorporation of high amount of titania into SBA-15, Mater. Res. Bull. 41 (2006) 436–447.
[30] M. Tasbihi, U. Lavrenčič Štangar, U. Černigoj, K. Kogej, Low-temperature synthesis and characterization of anatase TiO_2 powders from inorganic precursors, Photochem. Photobiol. Sci. 8 (2009) 719–725.
[31] N. Novak Tušar, A. Ristić, G. Mali, M. Mazaj, I. Arčon, D. Arčon, V. Kaučič, N. Zabukovec Logar, MnO_x nanoparticles supported on a new mesostructured silicate with textural porosity, Chem. Eur. J. 16 (2010) 5783–5793.
[32] S. Brunauer, P.H. Emmett, E. Teller, Adsorption of gases in multimolecular layers, J. Am. Chem. Soc. 60 (1938) 309–319.
[33] K.S.W. Sing, D.H. Everett, R.A.W. Haul, L. Moscou, R.A. Pirrotti, J. Rouquerol, T. Siemieniewska, Reporting physisorption data for gas/solid systems with special reference to the determination of surface area and porosity, Pure Appl. Chem. 57 (1985) 603–619.
[34] A. Sayari, P. Liu, M. Kruk, M. Jaroniec, Characterization of large-pore MCM-41 molecular sieves obtained via hydrothermal restructuring, Chem. Mater. 9 (1997) 2499–2506.
[35] B. Tan, H.-J. Lehmler, S.M. Vyas, B.L. Knutson, S.E. Rankin, Large- and small-nanopore silica prepared with a short-chain cationic fluorinated surfactant, Nanotechnology 16 (2005) S502–S507.
[36] E.P. Barrett, L.G. Joyner, P.P. Halenda, The determination of pore volume and area distributions in porous substances. I. Computations from nitrogen isotherms, J. Am. Chem. Soc. 73 (1951) 373–380.
[37] H. Einaga, S. Futamura, T. Ibusuki, Heterogeneous photocatalytic oxidation of benzene, toluene, cyclohexene and cyclohexane in humidified air: comparison of decomposition behavior on photoirradiated TiO_2 catalyst, Appl. Catal. B: Environ. 38 (2002) 215–225.
[38] T. Maggos, J.G. Bartzis, P. Leva, D. Kotzias, Application of photocatalytic technology for NO_x removal, Appl. Phys. A 89 (2007) 81–84.
[39] S.A. Larson, J.A. Widergren, J.L. Falconer, Transient studies of 2-propanol photocatalytic oxidation on titania, J. Catal. 157 (1995) 611–625.
[40] S. Senthilkumaar, K. Porkodi, R. Vidyalakshmi, Photodegradation of a textile dye catalyzed by sol–gel derived nanocrystalline TiO_2 via ultrasonic irradiation, J. Photochem. Photobiol. A: Chem. 170 (2005) 225–232.
[41] Y. Ohko, A. Fujishima, K. Hashimoto, Kinetic analysis of the photocatalytic degradation of gas-phase 2-propanol under mass transport-limited conditions with a TiO_2 film photocatalyst, J. Phys. Chem. B 102 (1998) 1724–1729.
[42] U. Lavrenčič Štangar, U. Černigoj, P. Trebše, K. Maver, S. Gross, Photocatalytic TiO_2 coatings: effect of substrate and template, Monatsh. Chem. 137 (2006) 647–655.
[43] V. Meynen, E. Beyers, P. Cool, E.F. Vansant, M. Mertens, H. Weyten, O.I. Lebedev, G. van Tendeloo, Post-synthesis deposition of V-zeolitic nanoparticles in SBA-15, Chem. Commun. (2004) 890–898.
[44] V. Meynen, P. Cool, E.F. Vansant, P. Kortunov, F. Grinberg, J. Karger, M. Martens, O.I. Lebedev, G. van Tendeloo, Deposition of vanadium silicate-1 nanoparticles on SBA-15 materials. Structural and transport characteristics of SBA-VS-15, Micropor. Mesopor. Mater. 99 (2007) 14–22.
[45] W.W. Lukens Jr., P. Schmidt-Winkel, D. Zhao, J. Feng, G.D. Stucky, Evaluating pore sizes in mesoporous materials: a simplified standard adsorption method and a simplified Broekhoff-de Boer method, Langmuir 15 (1999) 5403–5409.
[46] P.T. Tanev, L.T. Vlaev, An attempt at a more precise evaluation of the approach to mesopore size distribution calculations depending on the degree of pore blocking, J. Colloid Interface Sci. 160 (1993) 110–116.
[47] G. Munuera, F.S. Stone, Adsorption of water and organic vapours on hydroxylated rutile, Discuss. Faraday Soc. 52 (1971) 205–214.
[48] R.I. Bickley, G. Munuera, F.S. Stone, Photoadsorption and photocatalysis at rutile surfaces. II. Photocatalytic oxidation of isopropanol, J. Catal. 31 (1973) 398–407.